# Study of $e^+e^- \to D_s D^*_{s0}(2317)A$ process at BaBar+Belle

[1] **Dmytro Meleshko**, [1] Elisabetta Prencipe, [1] Soeren Lange, [2] Ashish Thampi
September 20, 2022

[1] Justus-Liebig-Universitat, Giessen, Germany,
[2] Forschungszentrum Jülich, Juelich, Germany

**DFG funded project:** "Search for four- and six-quark exotic states with c- and s- quarks"

EU grant n.822070

# Introduction

**Motivation:**

- Search for exotics is a hot topic: we do have evidence of more complicated structures than mesons and baryons;
- BaBar (1999-2008) and Belle (1999-2010) can still contribute;
- Many publications on the $X(4140)$&*co*. Still need clarification;

**Idea:**

- A combined data set (1.5 $ab^{-1}$) could allow to solve some *puzzling* cases;
- We propose to study $c\bar{c}s\bar{s}$ states (if any) in **different production mechanisms** and **different decay modes**, using the full data sets, on- and off- peak.

# Looking for exotic structures with $c\bar{c}s\bar{s}$ quarks

What are the possibilities?

Some examples

| Invariant mass system | Decay from: | Range [GeV/c$^2$] | |
|---|---|---|---|
| $D_s^- D_s^+$ | $B_s^0$ | [3.936 - 5.298] | $B_s^0 \to D_s^{(*)+} D_s^{(*)-} \pi^0$ |
| $D_s^- D_s^+ \pi^0$ | $B_s^0$ | [4.071 - 5.433] | |
| $D_s^- D_s^{*+}$ | $B_s^0$ | [4.080 - 5.433] | |
| $D_s^- D_{s0}^*(2317)^+$ | $B_s^0$ | [4.285 - 5.433] | |
| $J/\psi\phi$ | $B^0$ | [4.117 - 4.783] | $B^{0,\pm} \to J/\Psi\phi K^{0,\pm}$ |
| $J/\psi\phi$ | $B^\pm$ | [4.117 - 4.783] | |
| $J/\psi\phi$ | continuum | all range | $e^+e^- \to J/\Psi\phi$ + anything |
| $D_s^- D_{s0}^*(2317)^+$, $D_s^- D_s^+ \pi^0$, $D_s^- D_s^{*+}$ | continuum | all range | $e^+e^- \to D_s^{(*)+} D_s^{(*)-}$ + anything |

**Table 1:** Possible physics processes where one can search for $c\bar{c}s\bar{s}$ resonances.

# Prospects to study $D_sD_s^{(*)}$ in continuum

- First $e^+e^- \rightarrow D_s\pi^0X$ process studies:
  - BaBar: 1267 yield on 91 $fb^{-1}$
  - Belle: 761 yield on 87 $fb^{-1}$

Only $D_s^*(2317)$!

Extrapolation from the old analysis with $D_s^*(2317)$ only, but to the whole data sets:

- **BaBar @$\Upsilon(4S)$**: 5900;
- **Belle @$\Upsilon(4S)$**: 6226;

With one extra $D_s$ (e.g. +3 charged tracks), efficiency drops. BUT! We can use all $\Upsilon(nS)$ data sets!

- **Expected efficiency**: $< 1\%$.
  We expect 100-200 events on BaBar+Belle combined continuum dataset.
  **Sufficient statistics to study exotics!**

Why do we want to analyze $D_s^*(2317)$ in combination with $D_s$?
High potential discovery!

# $c\bar{s}$ spectrum puzzle

- Two more states were expected to be observed above $D^{(*)}K$ thresholds.
- Current $D^*_{s0}(2317)$ width UL value is 3.8 MeV;
- Below-1MeV potential improvement is expected;
- $D^*_{s0}(2317)$ width UL measurement is crucial in the attempts to reveal the nature of a state.

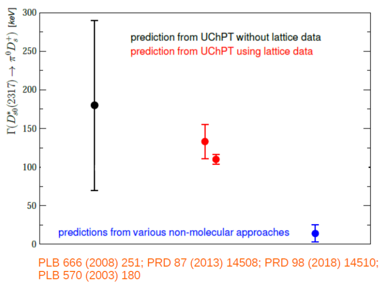


**Figure 1:** The $D_{s0}(2317)$ width predictions.

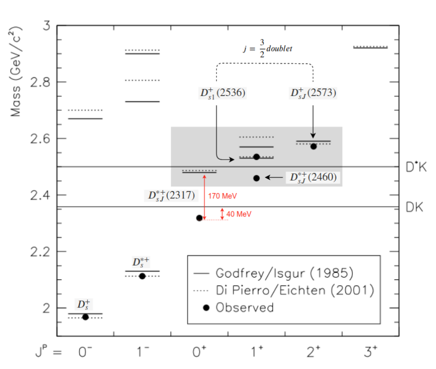


**Figure 2:** The $c\bar{s}$ meson spectrum.

arXiv:0710.1014v2 [hep-ex] 15 Oct 2007

| Reference | $D^*_{s0}(2317)^-$ width prediction (keV) | Interpretation |
|---|---|---|
| [12] | $6 \pm 2$ | pure $cs$-state |
| [13] | $7 \pm 1$ | pure $cs$-state |
| [14] | 10 | pure $cs$-state |
| [15] | 10 - 100 | tetraquark |
| [16] | $79.3 \pm 39.6$ | $DK$-molecule |
| [17] | 140 | Dynamically-generated resonance |
| [18, 19] | $133 \pm 22$ | $DK$-molecule |

**Table 2:** Major $D^*_{s0}(2317)$ width theoretical predictions summary.

# $D_s D_{s0}^*(2317)$ system study

# Signal MC. Signal generation and simulation

- 1 million events was generated for both decay channels;
- *Dpart* (D-particle) is an artificial particle that was manually added to evt.pdl. Formerly, the invariant mass assigned to the artificial state was equal to $M(D^*_{s0}(2317)) + M(D_s)$ and $M(D_{s1}(2460)) + M(D_s)$, respectively.

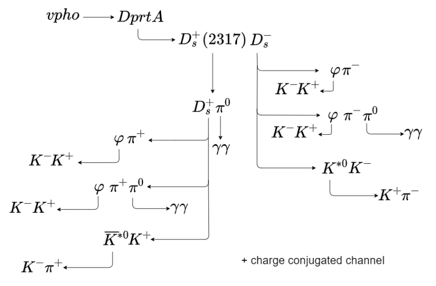


**Figure 3:** Signal MC. $D^*_{s0}(2317)$ decay scheme.

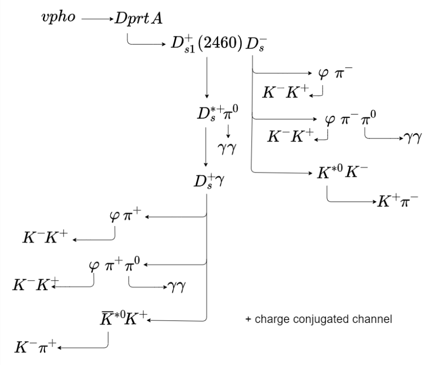


**Figure 4:** Signal MC. $D_{s1}(2460)$ decay scheme.

# Signal MC. Optimized selection and BCS implementation.

In addition to the selection summarized on the right, the BCS selection was applied in the latest iteration of a study.

Selection optimization study has been conducted.

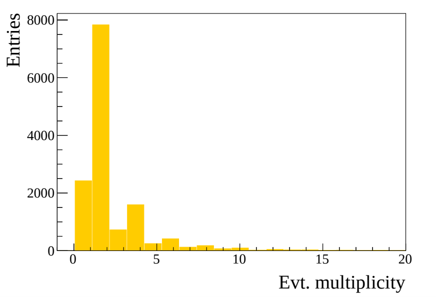


**Figure 5:** Signal MC. Event multiplicity before BCS application.

| Particle | Selection criterion |
|---|---|
| Tracks | $dr < 0.5$ cm<br>$dz < 3$ cm<br>$P_{K_1}(K/\pi) > 0.5$<br>$P_{K_2}(K/\pi) > 0.2$<br>$P_{\pi}(K/\pi) < 0.9$ |
| $\pi^0$ | $E(\gamma) > 100$ MeV<br>$p(\gamma\gamma) > 150$ MeV/c<br>$\chi^2(\gamma\gamma) < 200$<br>$122 < M(\gamma\gamma) < 148$ MeV/c$^2$<br>$P_{\chi^2}(\gamma\gamma) > 1\%$ |
| $\phi$ | $1.010 < M(KK) < 1.030$ GeV/c$^2$<br>$P_{\chi^2}(KK) > 0.1\%$ |
| $K^*(892)$ | $842 < M(K\pi) < 942$ MeV/c$^2$<br>$P_{\chi^2}(K\pi) > 0.1\%$ |
| $D_s$ | $1.9585 < M(D_s) < 1.9785$ GeV/c$^2$<br>$P_{\chi^2}(D_s) > 0.1\%$ |
| $D^*_{s0}(2317)$ | $p^*(D_s\pi^0) > 2.79$ GeV/c<br>$P_{\chi^2}(D_s\pi^0) > 0.1\%$ |
| Other | $\lvert cos\theta_H \rvert > 0.42$ |

**Table 3:** The summarized selection for $D_{s1}(2460)$ reconstruction.
$^*$ $\gamma_*$ denotes the photon combined with $D_s$ to create $D_s^*$ candidate decaying into $D_s\gamma$.

# Signal MC. Intermediate mesons reconstruction.

| Particle | M [MeV/c$^2$] | $\sigma_{Gaussian}$ [MeV/c$^2$] | $\sigma_{BW}$ [MeV/c$^2$] |
|---|---|---|---|
| $\pi^0$ | $135.31 \pm 0.09$ | $3.91 \pm 0.11$ | n/a |
| $\phi^0$ | $1019.4 \pm 0.1$ | $0.95 \pm 0.19$ | $4.10 \pm 0.24$ |
| $K^{*0}(892)$ | $893.4 \pm 0.5$ | $46.4 \pm 1.6$ | n/a |

**Table 4:** $\pi^0$, $\phi^0$ and $K^{*0}(892)$ invariant mass distributions fit parameters.

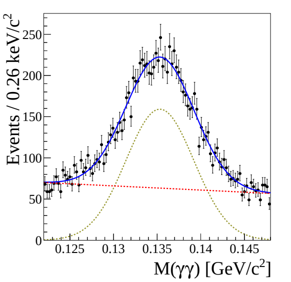


**Figure 6:** $\pi^0$ invariant mass distribution.

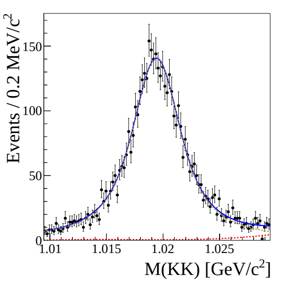


**Figure 7:** $\phi^0$ invariant mass distribution.

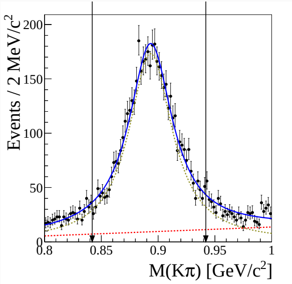


**Figure 8:** $K^{*0}(892)$ invariant mass distribution.

**Mass constraint fit is later applied.**

# Signal MC. $D_{sJ}$ mesons reconstruction.

**$D^*_{s0}(2317)$ true peak features:**

- $\sigma = 4.76 \pm 0.08$ MeV/c$^2$
  BaBar reference value (data): $8.6 \pm 0.4$ MeVc$^2$
- $\varepsilon = 0.245 \pm 0.005\%$

**$D_{s1}(2460)$ true peak features:**

- $\sigma = 5.07 \pm 0.13$ MeV/c$^2$
- $\varepsilon = 0.086 \pm 0.003\%$

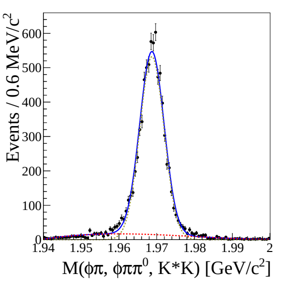


**Figure 9:** $D_s$ invariant mass distribution.

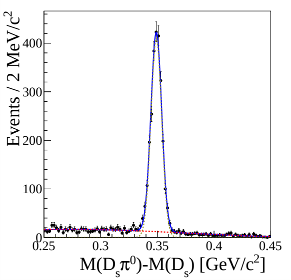


**Figure 11:** $D^*_{s0}(2317)$ invariant mass distribution.

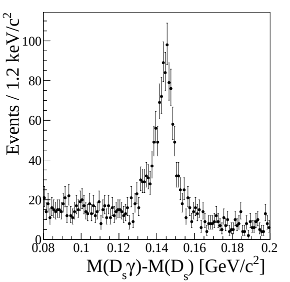


**Figure 10:** $D^*_s$ invariant mass distribution.

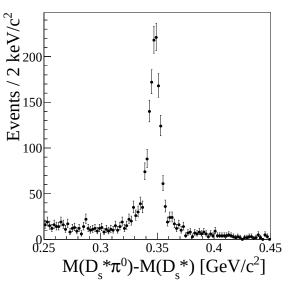


**Figure 12:** $D_{s1}(2460)$ invariant mass distribution.

# Signal MC. Reconstruction results analysis.

**The following information was shown in the Mikami note on "Observation of $D_{sJ}(2317)^+$ and $D_{sJ}(2460)^+$ in continuum".**

$D_{sJ}(2317)^+$ **invariant mass region:**

- *True $D_{sJ}(2317)^+$ peak:*
  $\sigma = 7.1 MeV,\ M = 2317 MeV;$
- *$D_{sJ}(2460)^+$ reflection peak (feed-down background):*
  $\sigma = 14.9 MeV,\ M = 2317 - 4 MeV$ Appears in generic MC.

$$f^{feed-down} = \frac{N_{feed-down}}{N_{true2317}} = 132\%$$

$D_{sJ}(2460)^+$ **invariant mass region:**

- *True $D_{sJ}(2460)^+$ peak:*
  $\sigma = 6.0 MeV,\ M = 2460 MeV;$
- *$D_{sJ}(2317)^+$ reflection peak (feed-up background):*
  $\sigma = 12.3 MeV,\ M = 2460 + 8 MeV$ Appears in generic MC;

$$f^{feed-up} = \frac{N_{feed-up}}{N_{true2460}} = 9.2\%$$

- *$D_{sJ}(2460)^+$ "broken signal":*
  $\sigma = 19.5 MeV,\ M = 2460 MeV$ Appears in signal MC.

$$f^{broken} = \frac{N_{broken}}{N_{true2460}} = 15.6\%.$$

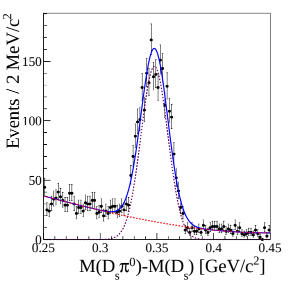


**Figure 13:** $D^*_{s0}(2317)$ invariant mass distribution acquired in reconstruction of the $D_{s1}(2460)$ signal sample

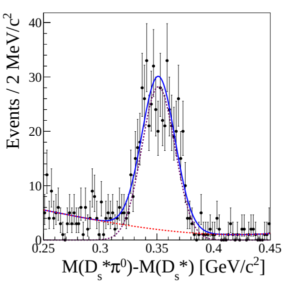


**Figure 14:** $D_{s1}(2460)$ invariant mass distribution acquired in reconstruction of the $D^*_{s0}(2317)$ signal sample

# Signal MC. Simultaneous fit.

$$f^{feed-down} = 2.529$$
$$f^{feed-up} = 0.254$$
$$f^{broken} = 0.141$$

$$\Delta M(D_s\pi^0) = N_1 G(\mu_1, \sigma_1)$$
$$\Delta M(D_s^*\pi^0) = N_2 G(\mu_2, \sigma_2) + f^{broken} N_2 G(\mu^{broken}, \sigma^{broken})$$

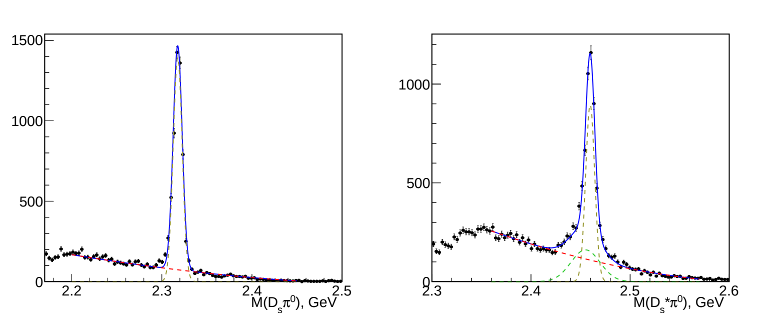


**Figure 15:** [left] $D_{s0}(2317)$ invariant mass distribution, [right] $D_{s1}(2460)$ invariant mass distribution. Red dashed curve is a background fitted with 3rd order polynomial, green dashed line is a "broken signal" fitted with Gaussian.

# Signal MC. $D_s D_{s0}^*(2317)$ system study (threshold case).

$$\varepsilon_{fin} = 0.22 \pm 0.02\%$$

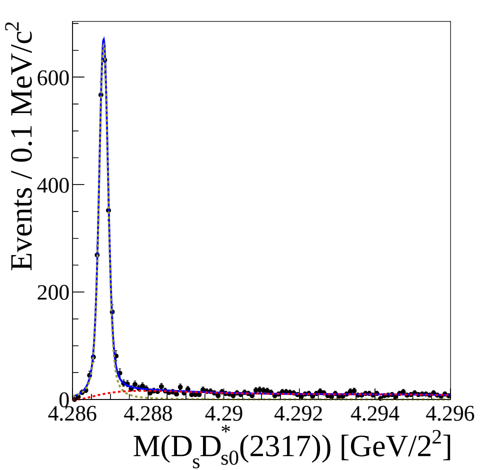


**Figure 16:** The $D_s D_{s0}^*(2317)$ invariant mass distribution in threshold case. The signal contribution is fitted by Voigt function, non-resonant background as approximated by the Threshold function.

# $c\bar{c}$ generic MC

# Generic MC. Simultaneous fit.

$$\Delta M(D_s\pi^0) = N_1 G(\mu_1, \sigma_1) + f^{down} N_2 G(\mu^{down}, \sigma^{down})$$
$$\Delta M(D_s^*\pi^0) = N_2 G(\mu_2, \sigma_2) + f^{up} N_1 G(\mu^{up}, \sigma^{up}) + f^{broken} N_2 G(\mu^{broken}, \sigma^{broken}) \quad (1)$$

ref: N = 3,843 $\pm$ 67, $\mu$ = 348.9 $\pm$ 0.1, $\sigma$ = 6.20 $\pm$ 0.10

ref: N = 835 $\pm$ 31, $\mu$ = 347.1 $\pm$ 0.2, $\sigma$ = 5.80 $\pm$ 0.20

Fit is consistent!

| Topology type | $\mu$, [MeV] | $\sigma$, [MeV] | N |
|---|---|---|---|
| True $D_{s0}^*(2317)$ signal | 349.3 $\pm$ 0.2 | 5.97$\pm$ 0.25 | 3,797 $\pm$ 137 |
| Feed-down background | 345.1 (fixed) | 13.5 (fixed) | $0.3297 \cdot N_2$ |
| True $D_{s1}(2460)$ signal | 347.1 $\pm$ 0.5 | 5.46 $\pm$ 0.60 | 811 $\pm$ 155 |
| Feed-up background | 352.0 (fixed) | 13.9 (fixed) | $3.042 \cdot N_1$ |
| $D_{s1}(2460)$ | 346.7 (fixed) | 22.7 (fixed) | $1.189 \cdot N_2$ |

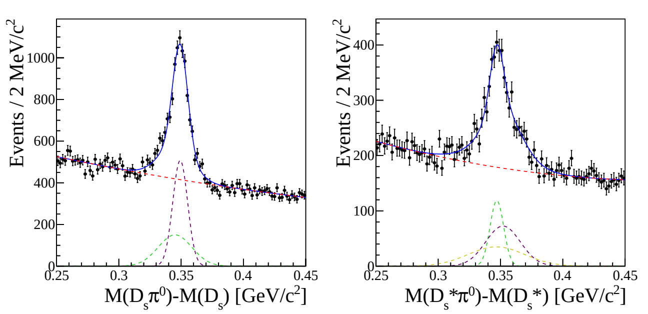


**Figure 17:** Simultaneous fit results: [left] $\Delta M(D_s\pi^0)$ distribution, [right] $\Delta M(D_s^*\pi^0)$ distribution. True peaks and corresponding reflection peaks are marked in these plots with the same color to visualize cross-feed effects.

# Generic MC. $D_s D_{s0}^*(2317)$ system study.

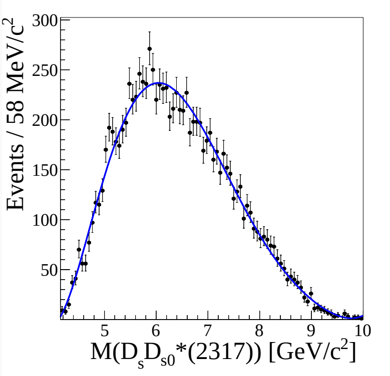


**Figure 18:** Belle. Generic MC. The $D_s D_{s0}^*(2317)$ invariant mass distribution.

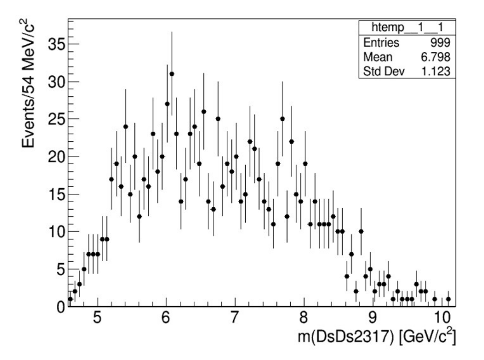


**Figure 19:** BaBar. Generic MC. The $D_s D_{s0}^*(2317)$ invariant mass distribution.

No enhancement is seen in both plots.

# Data

# Data. Simultaneous fit.

| Topology type | $\mu$, [MeV] | $\sigma$, [MeV] | N |
|---|---|---|---|
| True $D^*_{s0}(2317)$ signal | 350.1 $\pm$ 0.8 | 6.24$\pm$ 0.73 | 370 $\pm$ 45 |
| Feed-down background | 345.1 (fixed) | 13.5 (fixed) | $0.3297 \cdot N_2$ |
| True $D_{s1}(2460)$ signal | 349.2 $\pm$ 1.7 | 4.66 $\pm$ 1.17 | 68 $\pm$ 22 |
| Feed-up background | 352.0 (fixed) | 13.9 (fixed) | $3.042 \cdot N_1$ |
| $D_{s1}(2460)$ | 346.7 (fixed) | 22.7 (fixed) | $1.189 \cdot N_2$ |

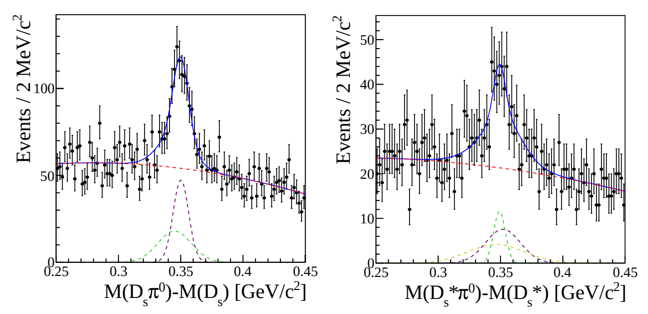


**Figure 20:** Simultaneous fit results on data: [left] $\Delta M(D_s \pi^0)$ distribution, [right] $\Delta M(D^*_s \pi^0)$ distribution.

# TMVA approach test

# MVA methods comparison

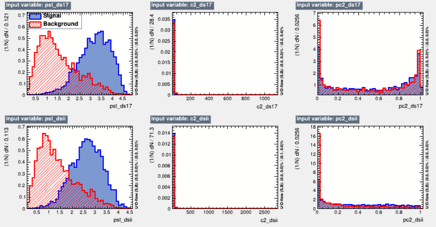


**Figure 21:** MVA input variables for signal (blue) and background (red) events.

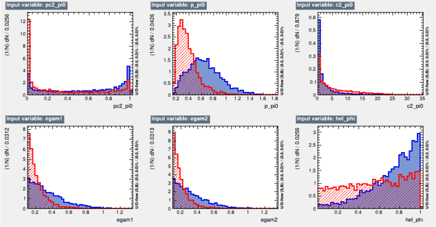


**Figure 22:** MVA input variables for signal (blue) and background (red) events.

- Pre-selection is applied.
- Performances of MLP, BDT, Fisher and DNN methods are compared → **MLP is chosen**
- Set of input variables is optimized with respect to correlation matrix → **redundant variables eliminated**.

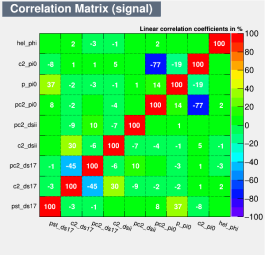


**Figure 23:** Input parameters Correlation Matrix for signal events.

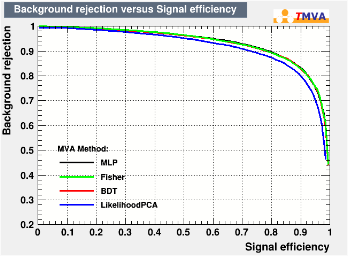


**Figure 24:** ROC curve.

# MLP application

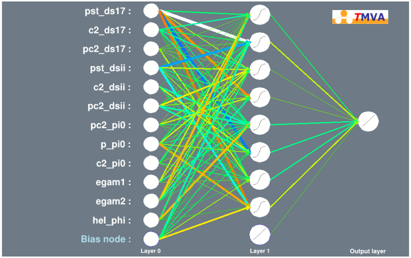


**Figure 25:** MLP architecture.

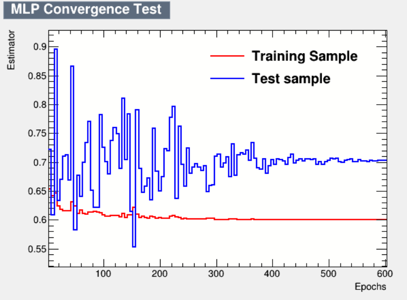


**Figure 27:** MLP convergence test.

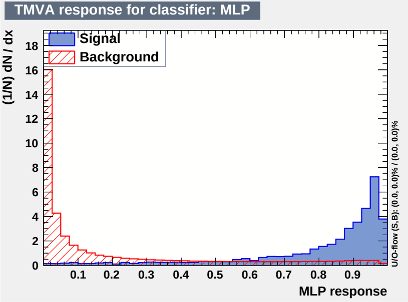


**Figure 26:** MLP response for classifier on training sample.

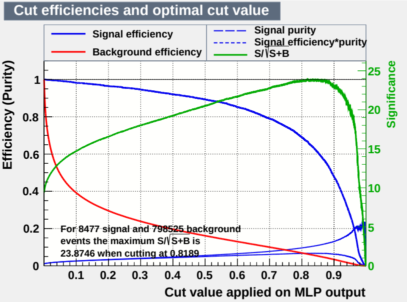


**Figure 28:** FoM dependence on classifier cut value.

# MLP application

Higher (x2) yield is reached!

| Topology type | $\mu$, [MeV] | $\sigma$, [MeV] | N |
|---|---|---|---|
| True $D^*_{s0}(2317)$ signal | $349.6 \pm 0.5$ | $7.16 \pm 0.59$ | $792 \pm 62$ |
| Feed-down background | 344.0 (fixed) | 13.4 (fixed) | $0.170 \cdot N_2$ |
| True $D_{s1}(2460)$ signal | $347.3 \pm 1.8$ | $6.98 \pm 1.72$ | $137 \pm 36$ |
| Feed-up background | 349.6 (fixed) | 14.6 (fixed) | $2.097 \cdot N_1$ |
| $D_{s1}(2460)$ broken signal | 345.5 (fixed) | 17.0 (fixed) | $0.231 \cdot N_2$ |

Cuts: $N(D^*_{s0}(2317)) = 370 \pm 45$ $N(D_{s1}(2460)) = 68 \pm 22$

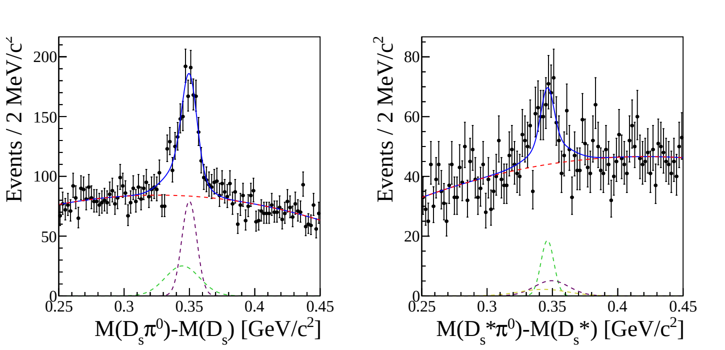


**Figure 29:** Simultaneous fit results on data selected with MVA: [left] $\Delta M(D_s\pi^0)$ distribution, [right] $\Delta M(D_s^*\pi^0)$ distribution.

# Look at $D_s D_{sJ}$ system on data (unblinded)

## Look at $D_s D_{sJ}$ system on data (unblinded)

- A tough mass cut and a mass constraint fit was applied on both primary $D_s$ mesons.

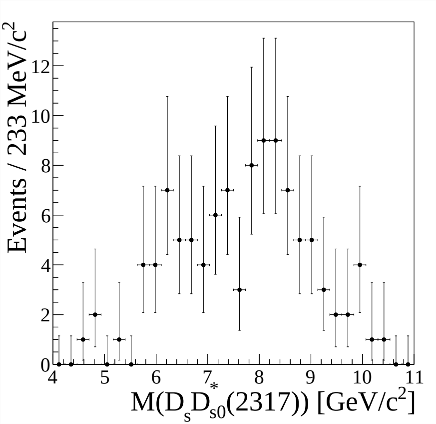


**Figure 30:** $D_s D^*_{s0}(2317)$ invariant mass on data.

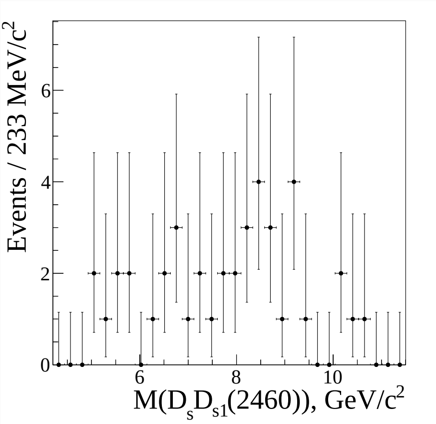


**Figure 31:** $D_s D_{s1}(2460)$ invariant mass on data.

# Look at $D_s D_{sJ}$ system on data (unblinded)

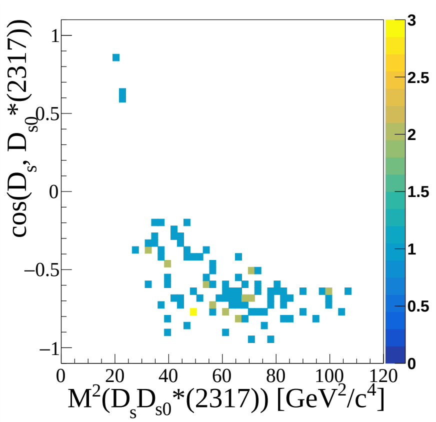


**Figure 32:** $D_s D^*_{s0}(2317)$ invariant mass on data.

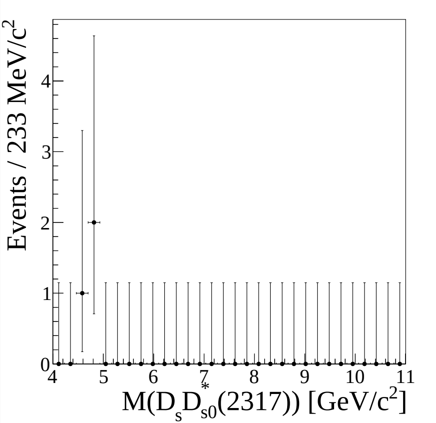


**Figure 33:** $D_s D_{s1}(2460)$ invariant mass on data.

## Curious to compare. First look at $X \to D_s D_{s1}(2536)$, $X \to D_s D_{s1}(2573)$.

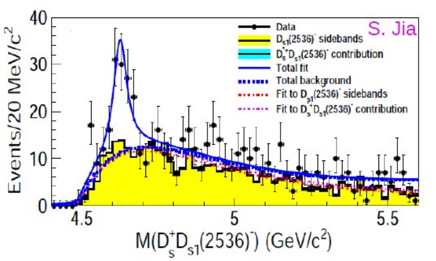


PRD 100 (2019) 111103

PRD 101 (2020) 091101

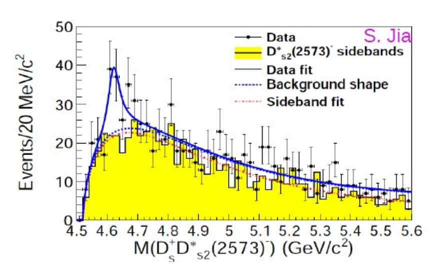


**$e^+e^- \to D_s D_{s1}(2536)$ via ISR**

- First observation of the Y(4620) $J^{PC} = 1^{++}$
- $5.9\sigma$ significance at 921.9 fb$^{-1}$ luminosity;

$M = 4625.9^{+6.2}_{-6.0}(\text{stat}) \pm 0.4(\text{syst})\ \text{MeV/c}^2$

$\Gamma = 49.8^{+13.9}_{-11.5}(\text{stat}) \pm 4.0(\text{syst})\ \text{MeV}$

$\Gamma_{ee} \times \mathcal{B}(\text{Y}(4626) \to D_s D_{s1}(2536)) \times \mathcal{B}(D_{s1}(2536) \to$
$\to \bar{D}^{*0} K) = 14.3^{2.6}_{-2.6}(\text{stat}) \pm 1.5\ \text{eV(syst)}$

Compatible with Y(4660)

**$e^+e^- \to D_s D_{s2}(2573)$ via ISR**

- Evidence of the Y(4620) $J^{PC} = 1^{++}$
- $3.4\sigma$ significance at 921.9 fb$^{-1}$ luminosity;

$M = 4619.8^{+8.9}_{-8.0}(\text{stat}) \pm 2.3(\text{syst})\ \text{MeV/c}^2$

$\Gamma = 47.0^{+32.3}_{-14.8}(\text{stat}) \pm 4.6(\text{syst})\ \text{MeV}$

$\Gamma_{ee} \times \mathcal{B}(\text{Y}(4620) \to D_s D_{s2}(2573)) \times \mathcal{B}(D_{s2}(2573) \to$
$\to \bar{D}^{0} K) = 14.7^{+5.9}_{-4.5}(\text{stat}) \pm 3.6\ \text{eV(syst)}$

# Progress summary and future plans

- Reconstruction efficiency for $D_s D_{s0}^*(2317)$: 0.22% after BCS.
- Simultaneous fit issue has been fixed.
- Selection optimization was conducted.
- MVA approach is optimized: impressive gain is reached!
- A precise $D_s^*(2317)$ Gaussian width measurement:
  - $\sigma(D_{s0}^*(2317)) = 7.16 \pm 0.59$ MeV/c$^2$
  - $\sigma(D_{s1}(2460)) = 6.98 \pm 1.72$ MeV/c$^2$
- A precise $D_{sJ}$ mass splitting measurement:
  - $\Delta M(D_s^*(2317)) = 349.6 \pm 0.6$ MeV/c$^2$ (PDG: $349.4 \pm 0.6$ MeV/c$^2$)
  - $\Delta M(D_s D_{s1}(2460)) = 347.2 \pm 1.9$ MeV/c$^2$ (PDG: $347.3 \pm 0.7$ or $349.1 \pm 0.6$ MeV/c$^2$)
- Systematic uncertainties evaluated.
- Belle Note v6 is delivered.
- Sideband study was performed.
- RC approved opening the box.
- A hint of a new structure is visible (yet to be studied deeper).
- There used to be technical errors that were preventing us from progressing in BaBar: it is fixed now, to be updated soon.

# Backup

# Looking for exotic structures with $c\bar{c}s\bar{s}$ quarks

- The proposal is to study the following decay modes in continuum:
  - $e^+e^- \to D_s^{(*)+} D_s^{(*)-} X$;
  - $e^+e^- \to D_s^+ D_s^{*-}(2317) X$;
  - $e^+e^- \to J/\Psi \phi X$;
- Why?

| | |
|---|---|
| $M = (4168.8 \pm 2.4) MeV/c^2$<br>$\Gamma = (22^{+8}_{-6}) MeV$ | $I^G(J^{PC}) = 0^+(1^{++})$ |
| $M = (4274^{+8}) MeV/c^2$<br>$\Gamma = (49^{+12}_{-6}) MeV$ | $I^G(J^{PC}) = 0^+(1^{++})$ |
| $M = (4506^{+16}) MeV/c^2$<br>$\Gamma = (92 \pm 29) MeV$ | $I^G(J^{PC}) = 0^+(0^{++})$ |
| $M = (4684 \pm 7) MeV/c^2$<br>$\Gamma = (87 \pm 8) MeV$ | $I^G(J^{PC}) = 0^+(1^{++})$ |
| $M = (4704^{+17}) MeV/c^2$<br>$\Gamma = (120 \pm 50) MeV$ | $I^G(J^{PC}) = 0^+(0^{++})$ |

from B decays

| |
|---|
| $M = (4351^{+5}) MeV/c^2$<br>$\Gamma = (13^{+18}_{-10}) MeV$<br><br>$I^G(J^{PC}) = 0^+(?^?)$ |

from $\gamma\gamma$ interaction

# Signal MC. $D_s D_{s0}^*(2317)$ system study.

**The following Dsprt biases were additionally studied:**

- **Case A:**
  direct decay;
- **Case B1:**
  M = 4.286 GeV/c$^2$, $\Gamma$ = 0 GeV, J=0;
- **Case B2:**
  M = 4.3 GeV/c$^2$, $\Gamma$ = 0 GeV, J=0;
- **Case B3:**
  M = 4.5 GeV/c$^2$, $\Gamma$ = 0 GeV, J=0;
- **Case B4:**
  M = 4.7 GeV/c$^2$, $\Gamma$ = 0 GeV, J=0;
- **Case B5:**
  M = 5.0 GeV/c$^2$, $\Gamma$ = 2 GeV, J=0;
- **Case B6:**
  M = 6.0 GeV/c$^2$, $\Gamma$ = 4 GeV, J=0;
- **Case B7:**
  M = 6.0 GeV/c$^2$, $\Gamma$ = 4 GeV, J=1.

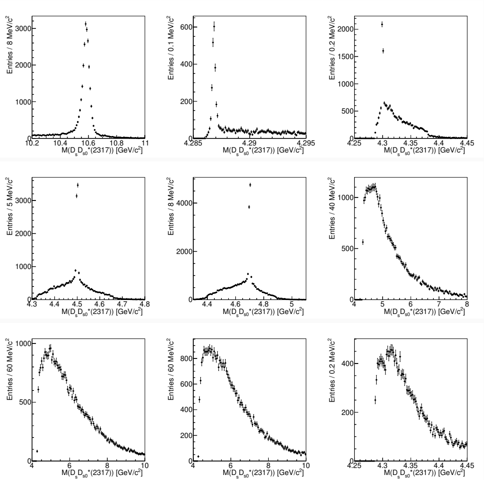


**Figure 34:** Signal MC simulation of the $D_s^+ D_{s0}^*(2317)^-$ invariant mass, where an artificial particle is introduced to the model in EvtGen. The simulation is performed over $\Upsilon(nS)$, n = 1, 2, 3, 4, 5, for the $e^+e^- \to D_s^+ D_{s0}^*(2317)^- X$ process and the following cases: A [upper-left], B1 [upper-central, B2 [upper-right], B3 [central-left], B4 [central-central], B5 [central-right], B6 [lower-left], B7 [lower-central] and B8 [lower-right].

# Generic MC. Selection optimization.

**Scaled momentum definition:**

$$x_p = \frac{p^*(D_s D_{s0}(2317))}{\sqrt{s - M^2(D_s D_{s0}(2317))}}$$

**$D_{s0}^*(2317)$ selection optimization:**

- $p^*(D_{s0}^*(2317)) > 2.79$ GeV/c
- $|cos\theta_H| > 0.42$

**$D_{s1}(2460)$ selection optimization:**

- $p^*(D_{s1}(2460)) > 3.05$ GeV/c
- $|cos\theta_H| > 0.44$

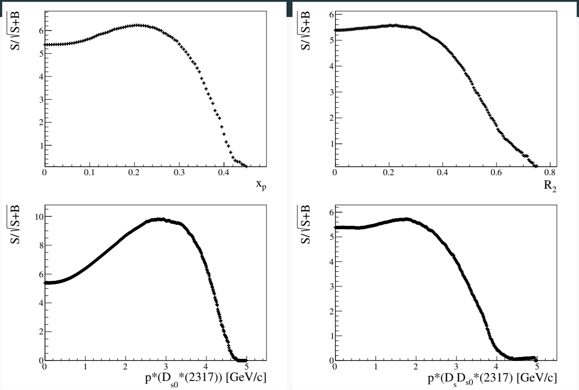


**Figure 35:** Generic MC. Selection optimization study for the competing selection criteria: [top-left] $x_p$, [top-right] $R_2$, [bottom-left] $p^*(D_{s0}(2317))$ and [bottom-right] $p^*(D_s D_{s0}(2317))$.

| Criterion applied | Yield | FoM |
|---|---|---|
| N/A | 6,476 | 5.384 |
| $x_P > 0.205$ | 4,157 | 6.231 |
| $R_2 > 0.225$ | 5,285 | 5.578 |
| $p^*(D_{s0}(2317)) > 2.79$ GeV/c | 4,538 | 9.813 |
| $p^*(D_s D_{s0}(2317)) > 1.79$ GeV/c | 4,018 | 5.721 |

**Table 5:** The $R_2$, $x_p$, $p^*(D_{s0}(2317))$ and $p^*(D_s D_{s0}(2317))$ optimized selection criteria effect comparison. The value FoM is evaluated as $S/\sqrt{S+B}$.

# Generic MC. $D_s^{(*)}$ mesons reconstruction.

**$D_{s0}^*(2317)$ true peak features:**

- $\sigma = 6.26 \pm 0.17$ MeV/c$^2$;
- $\mu = 348.9 \pm 0.2$ MeV/c$^2$;
- $N = 3855 \pm 80$.

**$D_{s1}(2460)$ true peak features:**

- $\sigma = 5.54 \pm 0.21$ MeV/c$^2$;
- $\mu = 347.4 \pm 0.3$ MeV/c$^2$;
- $N = 925 \pm 31$.

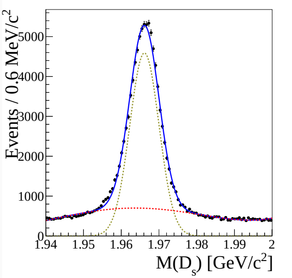


**Figure 36:** $D_s$ invariant mass distribution.

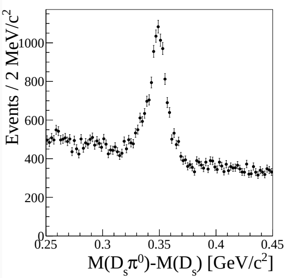


**Figure 38:** $D_{s0}^*(2317)$ invariant mass distribution.

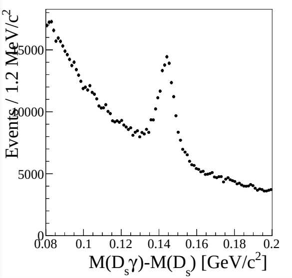


**Figure 37:** $D_s^*$ invariant mass distribution.

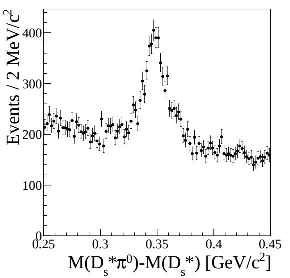


**Figure 39:** $D_{s1}(2460)$ invariant mass distribution.

# Sideband analysis

- **Signal regions [GeV/$c^2$]:**

$1.951 < M(D_s) < 1.981$

$0.123 < M(\pi^0)) < 0.145$

- **Sideband regions [GeV/$c^2$]:**

$1.905 < M(D_s) < 1.920$

$2.011 < M(D_s) < 2.026$

$0.090 < M(\pi^0) < 0.103$

$0.165 < M(\pi^0) < 0.178$

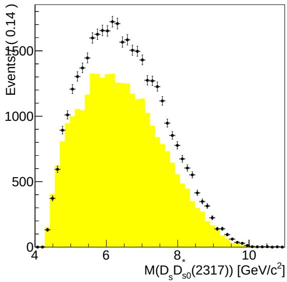


**Figure 40:** $D_s D^*_{s0}(2317)$ invariant mass distribution on generic MC: black points represent signal region, yellow histogram - sideband region.

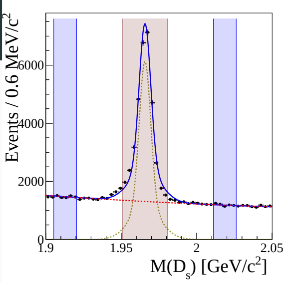


**Figure 41:** $\pi^0$ invariant mass distribution on generic MC: signal and sideband regions definition.

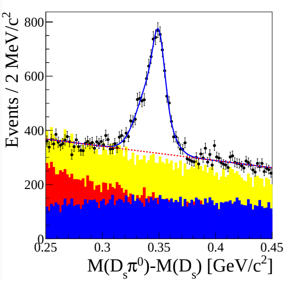


**Figure 42:** $D^*_{s0}(2317)$ invariant mass distribution on generic MC: black points indicate signal events; blue, red and yellow histograms indicate $D_s$, $\pi^0$ and total sideband events respectively.

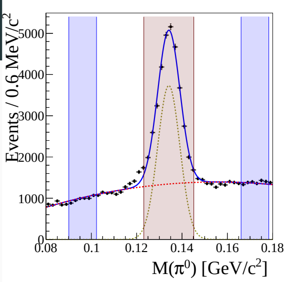


**Figure 43:** $\pi^0$ invariant mass distribution on generic MC: signal and sideband regions definition.

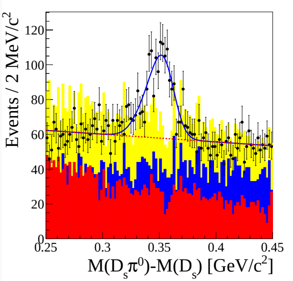


**Figure 44:** $D^*_{s0}(2317)$ invariant mass distribution on data: black points indicate signal events; blue, red and yellow histograms indicate $D_s$, $\pi^0$ and total sideband events respectively.

# Systematic uncertainties

**Contributing factors (calculated):**

- Charged tracks identification: 6 tracks;
- Track reconstruction;
- Efficiency uncertainty;

**Contributing factors (calculation is questionable):**

- MC model;

| Systematic error type (%) | | | |
|---|---|---|---|
| Charged tracks identification | Track reconstruction | Efficiency error | TOTAL |
| 3.21 | 2.10 | $4.69 \cdot 10^{-3}$ | 3.84 |

**Table 6:** Systematic uncertainties summary.

F. J. Dyson and N. H Xuong, Phys. Rev. Lett. 13 (1964) 815.

R. L. Jaffe, Phys. Rev. Lett. 38 (1977) 195.

R. Aaij et al (LHCb Coll.), Phys. Rev. Lett. 118 (2017) 022003.

R. Aaij et al (LHCb Coll.), Phys. Rev. D 95 (2017) 012002.

R. J. Eden et al, The analytic S-matrix, Cambridge University press (1966).

K. Guo et al., Phys. Rev. D91 (2015) 051504 (R).

F. Stancu, J Phys. G37 (2010) 075017.

R. F. Lebed and A. D. Polosa, Phys. Rev. D93 (2016) 094024.

D. Ebert et al., Phys. Lett. B 634 (2006) 214.

M. Karliner and J. L. Rosner, Nucl. Phys. A 954 (2016) 365.

C. P. Chen et al. (Belle Coll.), Phys. Rev. Lett. 104 (2010) 112004.

M. Nielsen, Phys. Lett. B634 (2006) 35.

P. Colangelo, F. De Fazio, Phys. Lett. B570 (2003) 180.

S. Godfrey, Phys. Lett. B568 (2003) 254.

A. Faessler et al, Phys. Rev. D76 (2007) 133.

M.F.M. Lutz and M. Soyeur, Nucl. Phys. A813 (2008) 14.

L. Liu et al, Phys. Rev. D87 (2013) 014508.

H.Y. Cheng and W. S. Hou, Phys. Lett. B566 (2003) 193.

M. Clevens et al., Eur. Phys. J. A50 (2014).

Private communication with Prof. Christoph Hanhart

Y. Mikami, et al. (Belle Coll.), *Measurements of the $D_{sJ}$ resonance properties*, arXiv:hep-ex/0307052.

Y. Mikami, et al. (Belle Coll.), *Measurements of the $D_{sJ}$ resonance properties*, arXiv:hep-ex/0307052v2.

B. Aubert, et al. (BaBar Coll.), *Observation of a Narrow Meson Decaying to $D_s + \pi^0$ at a Mass of 2.32 GeV/$c^2$*, arXiv:hep-ex/0304021.

D. Besson, et al. (CLEO Collaboration), *Observation of a Narrow Resonance of Mass 2.46 GeV/$c^2$ Decaying to $D_s^{*+}\pi^0$ and Confirmation of the $D_{sJ}^*(2317)$ State*, arXiv:hep-ex/0305100.

B. Aubert, et al. (BaBar Coll.), *A Study of the $D_{sJ}(2317)$ and $D_{sJ}(2460)$ Mesons in Inclusive $c\bar{c}$ Production Near $\sqrt{s} = 10.6$ GeV*, arXiv:hep-ex/0604030.

A. Zghiche, *Charm Meson Spectroscopy at BaBar and CLEO-C*, arXiv:0710.0314.

B. Aubert, et al. (BaBar Coll.), *Study of $B \to D_{sJ}^{(*)+}\bar{D}^{(*)}$ Decays*, arXiv:hep-ex/0408041v2.

L. Leskovec et al., Positive Parity D s Mesons, in 27th International Symposium on Lepton Photon Interactions at High Energy (LP15) Ljubljana, Slovenia, August 17-22, 2015, 2015.

S.-K. Choi, S.L. Olsen, K. Trabelsi, et al. (Belle Collaboration), *Bounds on the width, mass difference and other properties of $X(3872) \to \pi^+\pi^- J/\psi$ decays*, arXiv:1107.0163v1.